Analytica Chimica Acta 687 (2011) 114–128

Contents lists available at ScienceDirect

Analytica Chimica Acta

journal homepage: www.elsevier.com/locate/aca

Review

A review of monolithic multichannel quartz crystal microbalance: A review

Adisorn Tuantranont*, Anurat Wisitsora-at, Pornpimol Sritongkham, Kata Jaruwongrungsee

Nanoelectronics and MEMS Laboratory, National Electronics and Computer Technology Center, Pathumthani, Thailand

ARTICLE INFO

Article history:
Received 8 October 2010
Received in revised form
13 December 2010
Accepted 14 December 2010
Available online 21 December 2010

Keywords:
Monolithic multichannel quartz crystal microbalance
QCM array
Sensor array

ABSTRACT

Monolithic multichannel quartz crystal microbalance (MQCM) is an emerging technology for advanced sensing and measurement applications. In this report, a comprehensive review of MQCM technology is presented. Firstly, basic MQCM's design, simulation and characterization with emphasis on acoustic interference are described. Next, various MQCM schemes to minimize interference and enhance sensitivity of conventional MQCM devices based on modification of quartz substrate structure are digested. These include mesa, convex and *x*-axis inversion structures. Three important MQCM sensing platforms and their application areas are then discussed. These comprise MQCM as a static multichannel detector, series MQCM as a multichannel detector for the flow injection analysis and multi-frequency QCM for multi-sensitivity/multi-dynamic range detection. Finally, potential MQCM applications including electronic noses, bio-sensor arrays, and photocatatalytic measurement are illustrated and prospective MQCM applications including electronic tongues and electrochemical measurement are suggested.

Adisorn Tuantranont received the B.S. degree in electrical engineering from King Mongkut's Institute of Technology Ladkrabang, Thailand, in 1995, and the M.S. and Ph.D. degrees in electrical engineering from the University of Colorado at Boulder in 2001. Since 2001, he has been the director of the Nanoelectronics and MEMS Laboratory, National Electronic and Computer Technology Center (NECTEC), Pathumthani, Thailand. His research interests are in the area of micro electro-mechanical systems (MEMS), nanoelectronics, lab-on-a-chip technology and printed electronics. He has authored more than 50 refereed journals, 150 proceedings, and holds five patents. He also received the Young Technologist Award in 2004 from the Foundation for the Promotion of Science and Technology under the patronage of H. M. the King, Thailand.

Anurat Wisitsora-at received his Ph.D., M.S. degrees from Vanderbilt University, TN, U.S.A., and B. Eng. degree in electrical engineering from Chulalongkorn University, Bangkok, Thailand in 2002, 1997, and 1993, respectively. His research interests include microelectronic fabrication, semiconductor devices, electronic and optical thin film coating, sensors, and micro electromechanical systems (MEMS).

Pornpimol Sritongkham received her Ph.D. in electroanalytical chemistry from Cranfield University (United Kingdom) in 2002. Her current research is focused on the surface modification of QCM- and electrochemical biosensors and on the development of development of novel diagnostic devices.

Kata Jaruwongrungsee received the B. Eng. and M. Eng. degree in electronics engineering from King Mongkut's Institute of Technology Ladkrabang (KMITL), Thailand, in 2003 and 2005 respectively. Since 2006, he has been with the Nanoelectronics and MEMS Laboratory, National Electronics and Computer Technology Center (NECTEC), Thailand, as an assistant researcher. Presently, he is also doing his Ph.D. on electronics engineering at KMITL. His research is mainly focused on QCM based gas sensors and biosensors.

1. Introduction

Quartz crystal microbalance (QCM) is a thickness-shear mode bulk acoustic wave transducer that has been widely employed for physical, chemical and biological sensing applications [1–6]. QCM

* Corresponding author. Tel.: +662 564 6900x2111; fax: +662 564 6756.
E-mail address: adisorn.tuantranont@nectec.or.th (A. Tuantranont).

0003-2670/$ – see front matter © 2010 Elsevier B.V. All rights reserved.
doi:10.1016/j.aca.2010.12.022

devices derive from piezoelectric quartz crystal resonators that resonate electromechanically in a thickness-shear mode (TSM). Owing to piezoelectric effects, the resonant properties of crystal can be influenced by external physical loading, which may be classified into two main types, gravimetric and viscoelastic loading. In the first case, gravimetric force due to mass rigidly deposited on the crystal surface is balanced by a force originating from the shear gradient inside the crystal, leading to the resonance frequency shift (Δf_g), which is governed by Sauerbrey's equation [7,8]:

$$\Delta f_g = -\frac{2f_0^2}{\sqrt{\rho_q \mu_q}} \frac{\Delta M}{A} \quad (1)$$

$$f_0 = \frac{v}{2t_q} = \frac{\sqrt{(\mu_q/\rho_q)}}{2t_q} \quad (2)$$

where f_0 is the fundamental resonance frequency, ΔM is the mass deposited on QCM surface, A is the active electrode area, v is the acoustic wave velocity, ρ_q is the density of crystal (2.648 g cm^{-3} for quartz), μ_q is the shear modulus of the cut face (2.947×10^{11} g cm^{-1} s^2 for AT-cut quartz) and t_q is the crystal thickness. With this loading effect, QCM has been routinely used for thickness monitoring in physical vapor deposition processes.

For the viscoelastic loading, resonance frequency is changed due to acoustic-fluid damping interaction when QCM operates in viscoelastic medium such as liquid [9]. Unlike gravimetric loading, there are large changes of dissipation factor and resonant resistance due to energy losses of shear wave that travels through non-rigidly adsorbed layers [10–13]. The viscoelastic resonance frequency shift (Δf_v), dissipation factor change (ΔD) and resonant resistance change (ΔR) are given by:

$$\Delta f_v = -f_0^{3/2} \sqrt{\frac{\eta_L \rho_L}{\pi \mu_q \rho_q}} \quad (3)$$

$$\Delta D = 2f_0^{1/2} \sqrt{\frac{\eta_L \rho_L}{\pi \mu_q \rho_q}} \quad (4)$$

$$\Delta R = \frac{(2\pi \eta_L \rho_L f_0)^{1/2} A}{k^2} \quad (5)$$

where η_L, ρ_L and k are viscosity, density and electromechanical coupling factor of the liquid medium, respectively. Both dissipation factor and resonant resistance can be directly measured experimentally. The combined measurements of frequency shift and changes in the dissipation factor and resonant resistance have been termed, *QCM-D* and *QCM-R*, respectively [14]. With the combined mass and viscosity–density effects, QCM can be applied for bio/chemical sensing by coating with a chemically or biologically sensitive film to sense very small amount of adsorbed gases such as volatile organic compounds (VOCs) [15,16] and environmental pollutants [17–19] and liquid phase biochemicals. QCM/QCM-D evolves a solution measurement capability in analytical chemistry and electrochemistry applications due to wide detection range capability and very broad measurement applicability. Moreover, *electrochemical quartz crystal microbalance* (*EQCM*) variant, in which QCM is employed as a working electrochemical electrode, allows advanced electrochemical studies. Great amount of work relating to QCM/QCM-D/EQCM has been summarized in a number of review articles, which go over the utilization of QCM in analytical electrochemistry [20–22], QCM application areas in biosensors [23–29], drug discovery [6,30] and complex biopolymeric/biomimetic/biomolecular systems [1,4].

The main advantages of QCM in sensing fields include high sensitivity, high stability, fast response and low cost. In addition, it provides label-free detection capability for bio-sensing applications. However, QCM faces a major technical disadvantage of substantial characteristic dependence on environmental parameters particularly temperature. The problem can be partially alleviated by using AT-cut QCM surface (35.25° with respect to z-axis) because it has relatively low temperature coefficient compared to other well-characterized quartz crystal cuts [31]. Nevertheless, its performance is still not satisfactory for many sensing applications with largely varied environmental conditions. The environmental effects can be more effectively minimized by a dual QCM scheme [32–35], in which reference and sensing QCMs are employed. Both QCMs should have almost identical characteristic and present in the same environmental condition but reference QCM is prevented from sensing target species by the absence of sensing layer. The influence of environmental factors can be nullified out by taking the difference between them. In general, this scheme may be implemented in two ways. The first mean is to use a simple combination of two independent QCMs [32–35]. This method is found not to be very successful because QCMs made on different substrates can hardly be identical due to variation of crystal production. The QCM mismatch problem can be effectively eliminated by employing dual-QCM resonators on a single quartz substrate since two QCMs can be made highly identical [35]. However, the approach gives rise serious interference problems because acoustic wave induced by one QCM can interfere with the wave generated from the nearby QCM [36]. In addition, mass or stress loading on one QCM will induce spurious frequency shift on the other. The problems become particularly serious for two closely spaced identical QCMs [37].

Multiple QCM array system has been developed following the dual QCM scheme for advanced physical, chemical and biological sensing with environmental compensation [38]. In this system, one QCM is used as a reference and other QCMs are coated with different sensing layers. Multiple QCM array systems implemented by a simple combination of several independent QCMs are considered not suitable for general applications not only due to QCM mismatch problem but also bulkiness. Multiple microbalances on a single quartz substrate, commonly referred to as *monolithic multichannel quartz crystal microbalance* (*MQCM*), are thus considered highly promising. Moreover, the development of MQCMs leads to miniaturization of QCM devices because the size and spacing between QCMs are necessarily small as the array size increases. QCM miniaturization leads to additional benefits including lower cost, less sample/reagent consumption, faster sensing response and shorter diagnostic time [39]. Furthermore, QCMs in an array can be designed to have varying sensitivity, selectivity and dynamic range. Therefore, MQCM will be a versatile sensor platform with high performance and wide functionality. However, MQCM technology faces challenging strong acoustic interference problems that cannot easily be solved. It not only affects MQCM performance but also constrains the miniaturization.

In this report, a comprehensive review of MQCM technology is presented. Firstly, basic MQCM's design, simulation and characterization with emphasis on acoustic interference are described. Next, various MQCM schemes to solve the problems of conventional MQCM devices based on modification of quartz substrate structure are digested. These include mesa, convex and x-axis inversion structures. Three important MQCM sensing platforms and their application areas are then discussed. These cover MQCM as a static multichannel detector, series MQCM as a multichannel detector for the flow injection analysis, and multifrequency MQCM for multisensitivity/multi-dynamic range detection. Finally, potential and prospective applications for MQCM are illustrated.

2. Conventional MQCM

A conventional MQCM utilizes a few hundreds micron thick AT-cut quartz crystal plate with an array of electrode pairs deposited

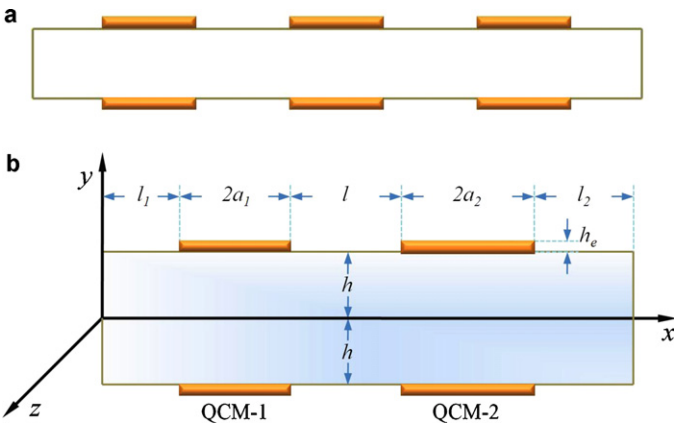

Fig. 1. Conventional MQCM (a) structure and (b) 2D model with generalized pair of QCMs [37].

on both sides as illustrated in Fig. 1(a). The size of electrode pairs and the spacing between them depend on the number and density of QCM in the array. In a MQCM system, acoustic wave induced by one QCM will propagate laterally through the substrate over a specific distance and if another QCM is located within vicinity of the acoustic field, acoustic interference will occur [40]. For a small MQCM array, spacing between adjacent QCMs may be sufficiently large and conventional MQCM structure can function properly since interference is negligible. For a large MQCM array, distance between adjacent QCMs must be small due to space limitation and hence strong acoustic interference is inevitable. The interference generally causes fundamental resonance frequency changes to all acoustically coupled QCMs and spurious frequency shifts due to mass or stress loading on neighboring QCMs. The problem becomes particularly serious when all QCMs are identical and operate at the same resonance frequency [37].

Acoustic interference in MQCM is highly complicated due to convolution of the simultaneous vibration motions from several resonators on one quartz plate. Additionally, it depends on several parameters of MQCM device including spacing between adjacent electrodes, geometry, dimensions and thickness of each electrode, mechanical and piezoelectric properties of quartz substrate and mechanical properties of electrode materials. Consequently, analysis of MQCM and its interference characteristics are mainly experimentally studied. Typically, interference between two adjacent QCMs is examined experimentally by impedance measurement of the two QCMs under exchanged external load and an electrical equivalent circuit is used to model and describes the response [36]. Electrical equivalent circuits including Butterworth–Van-Dyke (BVD) model [41] and transmission line representation [42] have been effectively used for QCM measurement analysis. Interference is introduced in a BVD circuit model by a complex coupling resistance between two BVD branches. In an equivalent circuit model, MQCM configuration is simplified into one-dimensional structure and the vibration profile is assumed to be uniform throughout the electrode surface. The results evaluated from these models are mainly valid in the region near the resonance frequency, which is calculated by applying Kirchhoff's law. Electrical circuit modeling can provide good estimation and prediction for experimental observation. However, it cannot give physical understanding and correlation between interference behaviors and physical parameters because it neglects some mechanical important features including modes coupling and energy trapping of electrode layer [40].

Theoretical modeling can provide insight understanding of interference mechanisms as well as relationship between interference behaviors and physical parameters. In general, theoretical analyses are performed on simplified models of complex real world problems so that analytical or semi-analytical solutions can be obtained. Recently, the theoretical analysis on interference of MQCM has been conducted using a simplified MQCM model with two generalized QCMs on a monolithic quartz crystal plate as illustrated in Fig. 1(b) [37]. This simple model is chosen to represent two nearest-neighbor QCMs in a monolithic MQCM array. Two quartz crystal microbalances, QCM-1 and QCM-2, are formed on an infinitely wide quartz plate ($l_1 = l_2 = \infty$) with a thickness of $2h$ and electrode widths of $2a_1$ and $2a_2$, respectively. The thickness of the electrode and separation between two QCMs are h_e and l, respectively. The analysis is based on one-dimensional modified Mindlin's theory with piezoelectric effect, which comprises a set of partial differential equations [43]. The effects of electrode sizes, spacing between two QCMs and QCM position on interference characteristics are extracted from the theoretical solutions.

The interference has been quantitatively characterized in terms of frequency interference (FI) and mass induce shift (MIS). FI is defined as the normalized frequency change $(\Delta\omega/\omega)_f$ of one QCM due to a mass loading on another while MIS $(\Delta\omega/\omega)_m$ is the normalized change in resonance frequency due to the adsorption of mass on its own electrode. MIS can be significantly modified due to the presence of neighboring devices in MQCM. FI and MIS are mathematically the same but they arise from different physical mechanisms. From the theoretical analysis, two parameters including relative width between two QCMs (a_2/a_1) and separation relative to QCM thickness (l/h) at a fixed QCM width relative to QCM thickness (a_1/h) are the most important factors that affect the FI and MSI.

FI is calculated from the resonance frequency shift of QCM-1 when the mass is placed on QCM-2. It is found from the simulation that FI has several peaks at different a_2/a_1 values. The largest FI for all a_1/h values occurs near $a_2/a_1 = 1$ where the two electrodes have the same width. This corresponds to the strongest fundamental acoustic coupling of QCMs operating at the same resonance frequency. At higher values of a_2/a_1, FI peaks for various QCM widths (a_1/h) appear at different c/a values. These peaks is attributed to anharmonic overtones excited from QCM-2 and coupled into QCM-1. The overtone coupling peaks $(a_2/a_1 > 1)$ periodically occurs at a_2/a_1 periods of ~1.7, 1.34 and 1.14 for $a_1/h = 10$, 20, and 40, respectively. Thus, strong interference occurs over a broader range of a_2/a_1 for smaller electrodes. On the other hand, anharmonic interference amplitudes of smaller electrodes are slightly lower than larger ones. Consideration of MIS offers an alternative perspective of interference. MIS is calculated from the resonance frequency shift of QCM-1 when the mass is placed on QCM-1 itself. It is seen from simulation that MIS decreases loaded frequency shifts by a factor of ~0.5 for both fundamental and anharmonic interference peaks. Thus, the mass sensitivity of QCM-1 is considerably reduced due to acoustic interference from QCM-2. In addition, MIS is found to slowly increase as electrode width (a_1/h) increases.

For the effect of separation, it is found that FI is high for small separations and then decreases rapidly with increasing separation as expected. In addition, FI for smaller electrodes is considerably higher than that for larger one and thus smaller electrodes require larger relative spacing. In contrary, MIS decreases slightly for small separations $(l/h < 5)$ and it is not strongly dependant on the separation for $a_2/a_1 = 0.5$. More recently, similar theoretical analysis on a more general MQCM model with an arbitrary number of QCMs on a monolithic quartz crystal plate is reported [44]. However, the analysis is limited to a special condition that all QCMs have the same electrode width and inter-electrode spacing and only the influences of the width and spacing on interference are evaluated. Some conclusions can be drawn from the theoretical analyses. Firstly, the microbalance channels of the devices may be designed to have different electrode sizes to avoid strong frequency interference.

Secondly, a large electrode size is helpful for acoustic energy trapping. However, the large size of electrode may also bring higher order modes and introduce higher order frequency interference. In applications, the size of electrode may be restricted by the number of channels mounted on quartz plate. Lastly, the separations need to be large to avoid strong frequency interference when all channels have the same size and same resonance frequency.

The theoretical calculation can provide insightful understanding of interference effects for MQCM and can be used to guide MQCM design. However, it cannot provide accurate prediction for real world 3D MQCM structures as 3D geometries such as edge effects of electrode layers and crystallographic orientation of electrode relative to quartz substrate cannot be directly included in the analysis. 3D simulation is thus required for more accurate design and analysis of MQCM devices. Recently, 3D simulation of a MQCM model with two symmetric QCMs on a monolithic quartz crystal plate has been reported [40]. The simulation is conducted using finite element analysis (FEA) method with the commercial software package, ANSYS. The ANSYS package provides electromechanical coupled field element, which includes piezoelectric effect. The full piezoelectric tensor formulation included in the package can account for anisotropic behaviors of piezoelectric crystals. 3D FEA simulation can thus provide considerably more quantitative information than 1D theoretical modeling. In addition to frequency interference, self-mass sensitivity and mutual-mass sensitivity, vibration mode shape and crystallographic orientation of an electrode pair can be obtained from 3D simulation results.

For example, 3D simulation reveals the phenomenon of resonance splitting into parallel and anti-parallel mode for a QCM pair when two identical QCMs operate at almost the same resonance frequency. In the 3D simulation model, the thickness of both gold electrodes and spacing between them are 6 mm, 100 nm and 3 mm, respectively. The parallel resonance (with f_1 = 4954960.1 Hz) results in the shear displacement overlapping of two QCMs, while antiparallel resonance (with f_2 = 49571192.6 Hz) causes the two QCMs to have opposite displacements. The displacement overlap in parallel resonance mode significantly induces acoustic coupling between two channels. With mass deposited on one QCM surface, both parallel and anti-parallel resonance frequencies decrease. Moreover, it is found that the parallel resonance frequency shift is linearly proportional to the mass absorbed while the anti-parallel resonance frequency shift non-linearly decreases and the sensitivity of the frequency shift for anti-parallel resonance decreases as the mass absorption per unit area increases. This results from the fact that the mass absorbed on one QCM results in asymmetrical detuning the two resonators and hence the splitting between the parallel and anti-parallel resonance frequencies increases.

Moreover, 3D simulation can provide the effect of anisotropic piezoelectric property of AT-cut quartz plate in x–z plane on interference. The coupling between a QCM pair is not the same for different angle θ to the x-direction as schematically shown in Fig. 2 because acoustic waves propagate with different velocities in different directions within the crystal plate. In this analysis, the interference is evaluated in term of mass–frequency influence coupling factor, which is defined by:

$$\alpha_{\mathrm{i}} = \frac{\psi_{\mathrm{i-j}}}{\psi_{\mathrm{i-i}}} \tag{5}$$

$$\psi_{\mathrm{i-j}} = \frac{\Delta f_{\mathrm{i}}}{\Delta m_{\mathrm{j}}} \tag{6}$$

where i and j are the labels of two QCMs, Δm_{j} is the mass per unit area added on the surface of QCM-j and Δf_{i} is the frequency shift of QCM-i. It is found from the analysis that the coupling strength is lowest when QCM pair (pair C_1–C_2 in Fig. 3) located in z-direction (θ = 90°) and the dependency on θ has two fold symmetry around x

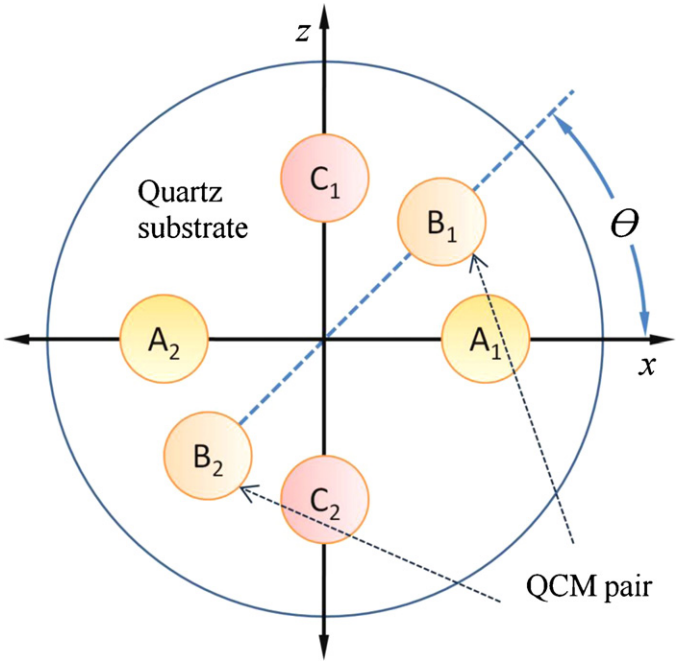

Fig. 2. Typical arrangements of QCM pairs in crystallographic z–x plane [40].

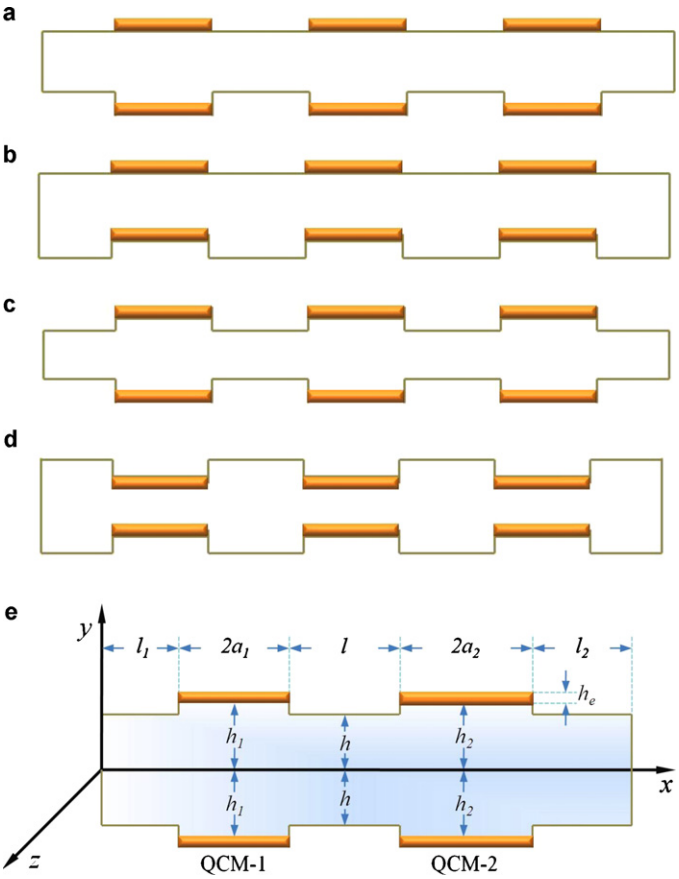

Fig. 3. Various mesa-shaped MQCM structures: (a) plano-mesa (b) plano-inverted-mesa (c) bi-mesa and (d) bi-inverted-mesa (e) 2D model with generalized pair of bi-mesa shaped QCMs [57].

and z axes. In addition, it is found that the frequency split between parallel and anti-parallel of QCM pair decreases as θ increases from 0° to 90°. The results indicate that the thickness shearing deformation transferred in x-direction of quartz crystal is more than that in z-direction. Therefore, QCM pair will be matched when their locations in x–z plane are at the same angle or 180° apart. This consideration should be taken into account in MQCM design. Interference among QCMs in conventional MQCM may be alternatively avoided by mean of successive oscillation or multiplexing. In this case, only one or a few QCMs can resonate at a time so that interference can completely be eliminated. This scheme is limited to applications, which do not require real-time or high speed measurement.

In addition to acoustic interference, other problems of conventional MQCM include spurious vibration, limited sensitivity and limited size of QCM electrodes. Spurious vibration occurs due to coupling between thickness shear (TS) and other modes including thickness flexural (TF), face shear (FS), thickness twist (TT) and higher order modes. The coupling between TS and TF occurs due to crystal edge effect and it is strong because both modes have a similar displacement field [45]. The coupling between TS and FS or TS and TT is relatively weak. In addition, the shear rotation about the z-axis is more than an order of magnitude less than the shear rotation about the x-axis or deflection in the y-direction [46].

Other important problems of MQCM are the limitation of sensitivity and electrode size. The mass sensitivity and diameter of MQCM electrode are both limited by the thickness of the crystal. The sensitivity is proportional to the square of resonance frequency, which is inversely proportional to quartz thickness. The thickness of quartz crystal is limited to around 100 μm because thinner quartz plates are too fragile and cannot be practically processed. The thickness constraint also limits diameter of electrode because small-diameter electrode QCM does not resonate or resonates with a very low Q factor if the diameter of the electrode to thickness of the crystal ratio is below 5 [47]. This limits miniaturization of conventional MQCM devices.

3. MQCM based on modified quartz substrate structure

Several methods have been developed to eliminate or minimize interference and other problems of conventional MQCM. Modification of quartz substrate structure is found to be the most effective approach to solve the problems. In this section, various MQCM schemes based on modification of quartz substrate structure will be described.

3.1. MQCMs with mesa shape designs

The most basic concept for minimizing the coupling of acoustic energy between adjacent QCMs is to increase the difference of the resonance frequencies between the electrodes and inter-electrode portions of the quartz plate. A direct way to increase the resonance frequency difference is to vary the quartz thickness between the electrode and inter-electrode regions. This can practically be done by means of standard micromachining process. The structure with varying quartz thickness in steps are commonly termed, *Mesa*, which can be subdivided into plano-mesa [48,49], plano-inverted-mesa [50,51], bi-mesa [48,49,52] and bi-inverted-mesa [53] as defined in Fig. 3. For plano-mesa structure (Fig. 3(a)), square cavity with reduced quartz thickness is formed in the inter-electrode regions while the other side is still planar. On the other hand, square trenches are created in the electrode regions for plano-inverted-mesa structure (Fig. 3(b)). For bi-mesa and bi-inverted-mesa structures (Fig. 3(c–d)), square cavities are made symmetrically on both sides.

The interference and acoustic energy trapping behaviors of the quartz mesa structure of different designs have been experimentally demonstrated [49,54]. It has been shown that the acoustic energy of the thickness shear mode of mesa-shaped MQCMs is considerably better confined within electrode regions than that of conventional MQCM and the separation between two adjacent resonators can substantially be reduced using mesa-type MQCM. With inverted-type-mesa designs, QCM resonators can operate at higher resonance frequency than those of non-inverted designs because the quartz plate thickness in the electrode area is decreased [51,53,55,56]. This scheme can thus solve the limitation of mass sensitivity of conventional MQCMs. Comparing between bi-mesa and plano-mesa schemes, QCMs with bi-mesa designs exhibit better resonance characteristics with lower spurious vibration mode and higher Q-factor than plano-mesa configuration because of the symmetric structure [48]. However, plano-mesa scheme are more practical than bi-mesa structure because fabrication process is considerably simpler and its top planar surface is more suitable for most applications than step-profile surface [38]. Therefore, plano-inverted-mesa structure has become more commonly used in MQCM devices.

Recently, bi-mesa MQCM has been theoretically analyzed [57,58] based on two-dimensional modified Mindlin's theory, which has also been used for analysis of conventional MQCMs. Two generalized mesa-shaped QCMs on a monolithic quartz crystal plate as illustrated in Fig. 3(e) are used as model to represent two adjacent QCMs in MQCM structures. Two quartz crystal microbalances, QCM-1 and QCM-2, are formed on surfaces of two mesas with quartz thickness of $2h_1$ and $2h_2$, mesa widths of $2a_1$ and $2a_2$, and distances to edges of l_1 and l_2, respectively. The thickness of the electrode, quartz thickness outside electrode regions and separation between mesas are h_e, $2h$ and l, respectively. In this analysis, the Mindlin's equations for the coupled vibrations of TS and TF modes are used and piezoelectric effect is neglected. The kinetic and potential energies per cycle in the different portions of the mesa structure are computed. The kinetic energy consists of deflective and rotational kinetic energies while the potential energy contains rotational and extensional potential energies.

The interference behaviors of mesa shaped MQCM are evaluated in terms of frequency interference (FI) described in the previous section and normalized energy-trapped of QCM-1, which is defined as the ratio of energy trapped within QCM-1 section to the total energy in the quartz plate. The effects of mesa height, electrode sizes, spacing between two QCMs and QCM position on interference behaviors are acquired from the theoretical calculation. The heights of the two mesas, h_1 and h_2, are both equal to h_m. It is shown that FI decreases monotonically with increasing mesa height for the infinite plate case. When the plate has a finite length, FI graph still follows the same curve but periodical spikes occur. These spiking peaks correspond the coupling of TF and TS modes due to the existence of boundaries. It is found that a small relative mesa height ($h_m/h > 1.03$) can effectively reduce frequency interference between two adjacent QCMs. Thus, only small etching depth is needed to form mesa structure with low interference and this can considerably simplify mesa-MQCM fabrication process. However, strong coupling regions due to the presence of a boundary still exist for mesa structure with specific relative heights and thus they must be avoided in the mesa-MQCM design.

In this analysis, the energy trapped in QCM structure has been considered with different MQCM parameters. The energy trapped in QCM-1 is determined when only QCM-1 is under excitation. For mesa-MQCM with above parameters, energy trapped in QCM-1 is found to increase as relative mesa height increases and negative peaks, where the trapped energy decreases markedly, also appear at the same relative mesa height as those of FI. At these peaks, nearly half of the energy is found to escape to other parts of the plate in

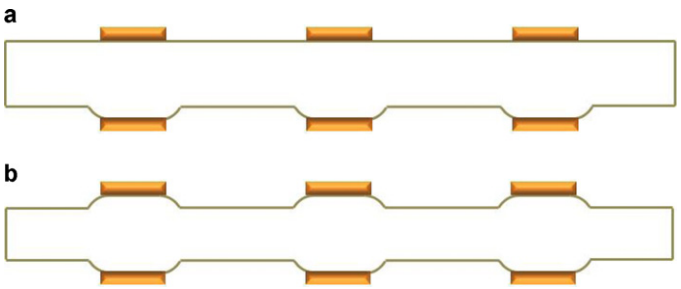

Fig. 4. Various convex-shaped MQCM structures: (a) plano-convex and (b) bi-convex.

the form of a flexural wave [58]. The effect of the relative electrode width (a_2/a_1) on energy trapped in QCM-1 for mesa and no mesa structures is also analyzed. It is shown that only small relative mesa height of 1.02 can considerably increase energy trapped in QCM-1 except the regions near the peaks of fundamental ($a_2/a_1 = 1$) and anharmonic coupling ($a_2/a_1 > 1$). At the peaks of coupling regions, the maximum loss from QCM-1 can be half of the total acoustic energy and most of the escaping energy is trapped in QCM-2. The main benefits of the mesa structure are to narrow the range of strong coupling region and reduce interference outside these regions. These give considerable flexibility for the design of MQCM devices.

3.2. MQCMs with convex shape designs

Mesa design can offer considerable improved MQCM performance in terms of interference reduction and sensitivity enhancement. However, the straight edge mesa structure cannot effectively correct mode coupling problems between the fundamental TS and spurious modes [54]. As discussed in the previous section, the coupling between TS and TF modes remains quite substantial in mesa-shaped MQCM. The coupling is undesirable because energy is taken from the usable frequency vibration, resulting in damping and lower *Q*-factor. High *Q*-factor is important for ultra sensitive detection in liquid mode. Several structures including dual-step mesa [54], multi-step mesa [59] and spherical convex [47,60–62] have been developed to reduce mode coupling problems so that oscillation energy is better trapped at the center and very little dissipation occurs at edges. Among these, the spherical convex-shape structure can theoretically separate vibrating modes most effectively. Spherical convex-shaped MQCMs, which include plano-convex [60] and bi-convex [47,61] designs as illustrated in Fig. 4, have been reported.

Some sophisticated processes have been developed to realize convex-shaped 3D QCM structures. Firstly, planoconvex quartz-crystal unit is fabricated based on a laborious mechanical polishing method [60]. Recently, the miniaturized beveled bi-convex QCM has been developed by photoresist thermal melting [61] and photoresist reflow with solvent vapor process [47]. The later process is particularly promising because diameter, curvature and height of spherical convex shape can be well controlled with moderate cost and reproducibility. In this process, spherical shaped photoresist on quartz substrate is formed after photolithographic patterning and reflow in a suitable organic solvent. Reactive ion etching in SF_6/Xe gas mixture [61] is then used to transfer spherical structure into quartz-crystal substrate. Spherical bi-convex MQCM structures with diameter ranging from 100 μm to 2 mm and height from 1 to 7 μm have been realized and the resonant characteristics have been studied.

It has been demonstrated that the spherical bi-convex QCM exhibits very sharp resonant peak with negligible spurious vibrating modes while the planar QCM resonates with numerous spurious vibration [47]. The spherical convex-shape can effectively decouple the vibrating modes in QCM. An optimum *Q*-factor of ~80000, which is twice higher than that of the 100 μm-thick planar QCM, is obtained from the spherical convex shape with diameter and height of 2 mm and 1.7 μm, respectively. The spherical bi-convex and planar QCM are also studied in viscoelastic liquid using glycerol/water mixtures contacted on one side of QCM. It is shown that the effective loading range of the spherical bi-convex QCM is considerably larger than that of the planar QCM. The effective loading range in liquid is defined as the range in which the resonance frequency shift is linearly proportional to $(\rho\eta)^{1/2}$ where ρ and η are liquid density and viscosity, respectively. In addition, the maximum viscosity in the effective region for the spherical biconvex QCM is found to be approximately five times greater than that for the planar QCM.

3.3. MQCMs with x-axis inversion

x-Axis inversion [63–65] is a useful method that can increase the difference of the resonance frequencies between the electrode and inter-electrode portions of the quartz plate. An advantage of this technique is that it does not require physical removal of quartz material from the plate. It is the phenomenon that *x* crystallographic axis of quartz crystal is locally rotated by 180° under a specific thermal treatment as illustrated in Fig. 5(a). In the treatment process, an AT-cut plate is coated with a thin Cr or NiCr film on a desired pattern and then heated at 520–560 °C in a vacuum. *x*-Axis inversion would occur only in the area under the metal film because of mechanical stress induced by thermal expansion difference between the quartz plate and the film. In the inversion area, the *y*-axis is also inverted and the cut angle changes from $+\theta$ to $-\theta$ AT-cut. Alternatively, *x*-axis inversion can be formed by applying heating current to the metal film [63]. In this case, heat is more concentrated on the patterned metal film and *x*-inversion can occur at a relatively low temperature of 480–500 °C with DC current density of 13.3–16.7 mA mm^{-2}. This method is advantageous due to relatively low process temperature but it requires additional electrical connection, which can be cumbersome for complex patterns. Lastly, laser has been applied to selectively induce *x*-axis inversion in the metal film [65]. The advantages of this method are that it requires lower substrate temperature of 400–480 °C and *x*-axis inversion area can be defined with higher lateral resolution, allowing narrower *x*-axis inversion region and hence higher MQCM density.

x-Axis inverted area exhibits different dispersion characteristics of the elastic wave propagation from non-inverted one. It is found that the cut-off frequency of the *x*-axis inverted area is higher than that of the non-inverted area by a factor of 1.47. As a result, plate wave excited at the electrode area is highly attenuated as it propagates into the *x*-axis inverted area. The attenuation of the wave in the *x*-axis inversion area is proportional to the ratio of *W* and *H*, where *W* is the width of the *x*-axis inversion area and *H* is the plate thickness. From theoretical calculation, attenuation is estimated to be more than 70 dB for $W/H = 3$. Thus, adjacent resonators can be effectively mechanically isolated by an interposed x-axis inverted region and *x*-axis inversion is promising for acoustic decoupling in MQCM device.

MQCM structure with *x*-axis inversion has been proposed as illustrated in Fig. 5(b) [63]. In the structure, *x*-axis inversion areas are formed in the space between adjacent QCM electrodes. *x*-Axis inversion area is created by Cr film deposition and the thermal treatment. Quartz surface is then lightly etched by buffered oxide etching solution and Cr film is etched away, leaving the pattern of *x*-axis inverted regions on substrate. Finally, QCM electrode film is deposited by sputtering or evaporation and pattern of electrode array is aligned to the *x*-axis inverted pattern by standard photolithography. The acoustic decoupling between two adjacent

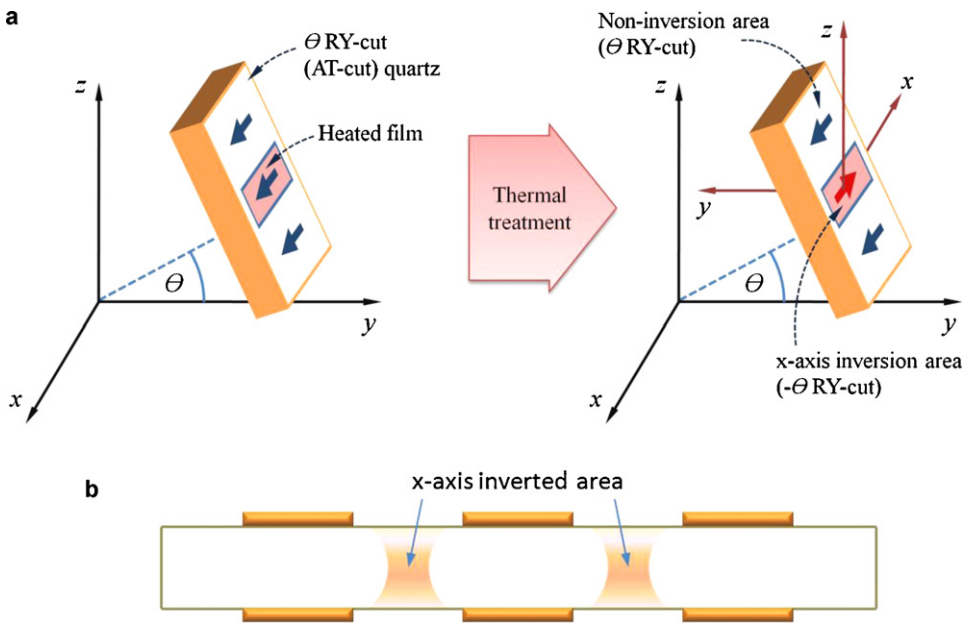

Fig. 5. *x*-Axis inversion: (a) schematic of inversion process [63] and (b) *x*-axis inverted MQCM structure [35].

QCMs separated by *x*-axis inversion region has been experimentally demonstrated by mean of two-port network measurement. In the measurement, ac input is applied to the first QCM at port 1 while both electrodes of the second QCM at port 2 are either open or short and impedance–frequency response of the first QCM is measured. For a conventional MQCM, one resonant peak occurs when port 2 is open while two resonant peaks appear at different frequencies when port 2 is short. This indicates the mechanical coupling between two resonators under the short circuit condition. On the other hand, the frequency response of the first QCM is not affected by the termination of the second QCM of MQCM with *x*-axis inversion, demonstrating that both resonators are effectively isolated by the *x*-axis inversion area.

Table 1 summarizes advantages, disadvantages and available reported references and parameters [7,36,38,39,47,62,65–82] of all MQCM structures discussed in the preceding sections. It is evident that the common advantage of all MQCM structures with modified quartz substrate is low interference that allows large array size and high array density. In addition, inverted-mesa structures offer specific advantages of higher resonance frequency and mass sensitivity because of reduced thickness of active quartz layer while convex and bi structures can reduce TS–TF and TS–extension mode couplings, respectively. However, MQCM structures with modified quartz substrate are still not widely employed because they involve difficult fabrication processes including deep etching, thermal treatment and aligned electrode patterning. In particular, all bi structures have rarely been reported because of very intricate two-side processing and incompatibility with flow injection system. Among MQCM with modified quartz substrate, plano-inverted-mesa has been the most frequently reported structure because it simultaneously offers low interference, high resonance frequency, high mass sensitivity and compatibility with flow injection system while its fabrication is not more difficult than those of others in its category and its frequency mode coupling can be minimized by employing suitable design.

4. MQCM sensing platforms

An array of QCMs may be formed differently into a variety of MQCM sensing platforms for various types of sensing or measurement applications. In this section, potential MQCM sensing platforms will be explained [38].

4.1. MQCM as a static multichannel detector

In this platform, identical QCMs in an array are coated with different sensing layers or receptors and MQCM is set in a simple sample cell as illustrated in Fig. 6. Additionally, one channel of MQCM should be used as a reference, which has no receptor, to compensate for the influences of the temperature, viscosity, and density of medium. In these cases, simple measurements with one drop of an electrolyte solution without an electrolytic cell are also possible [38]. Different receptors will accept additional mass from target species by means of binding, adsorption or deposition causing resonance frequencies of underlying QCMs to change accordingly.

The main class of applications for this platform is multi-component analysis, which is used to identify a multi-component mixture and/or its ingredients with respective concentrations. There are three main schemes for multi-component analysis. Firstly, QCMs are bound with different receptors, which are selective to individual component in the target mixture. The resonance frequency shift of QCM coated with each receptor can be used to directly identify the presence of each component and determine its concentration. The scheme can work only when receptors with very high specificity to target species are available. Existing receptors with such a specific property include complementary DNAs and antigen/antibody [5,27,83]. Thus, this technique can only be applied to some specific biosensing while it cannot generally be implemented for chemical and gas sensing.

The second scheme employs a group of different receptors on QCMs that have low selectivity towards a set of components in the mixture. When receptors are exposed to target components, they respond differently according their selectivity, producing resonance frequency shifts to related QCMs. The presence and concentrations of all target components are then determined from recognized relationships of selectivity parameters of all components. The number of different receptors should be the same as the number of components to obtain unique deter-

Table 1
Summary of advantages, disadvantage and available reported parameters (up to September 2010) of MQCM structures.

MQCM structure		Advantages	Disadvantages	Available reported parameters (up to November 2010)		
				References	f_0 (MHz)	Array size
Conventional		Very simple and low cost fabrication process	Highly susceptible to interference	Interference characteristic of two channel MQCM [36]	5	2
			Limited resonance frequency, array size and density, mass sensitivity	MQCM for ammonia and humidity sensing [66]	10	6
			Strong frequency mode couplings	MQCM coated with silica hybrid films for gas sensing application [67]	5,6	4
				Comparative study between QCM and MQCM in humidity sensing application [68]	10	4
				MQCM with multiplexed oscillator for VOC sensing [69]	10	4
				Analysis of MQCM with circular flow chamber [70]	5	4
				MQCM coated with ionic liquids films and conductive polymer for VOCs detection [71]	10	4
				MQCM coated with MIP for detection of yeast cells in liquid [72]	10	4
				ACR type MQCM for immunoglobin detection [73]	17	2
				MQCM for sensing terpenes in fresh and dried herbs [74]	10	6 (3 × 2)
Mesa	Plano-mesa	Low interference	Required difficult deep etching process	n/a	n/a	n/a
		Large array size and density	Limited resonance frequency, mass sensitivity, electrode size			
			Some remaining frequency mode coupling particularly TS–TF and TS–extension			
	Plano-inverted-mesa	Low interference	Required difficult deep etching process	Multi-frequency MQCM for toluene detection [7]	20–50	16
		High resonance frequency, array density, mass sensitivity	Some remaining frequency mode coupling particularly TS–TF and TS–extension	MQCM possibility to 2D mass mapping [38]	10	4
				Multi-frequency MQCM for VOC sensing [75]	20	6
				MQCM coated with SW-CNT for gas detection [76]	n/a	9
				MQCM coated with SAM for HAS detection [77]	27	9
				MQCM functionalized for avidine and BSA detection [79]	62	9
	Bi-mesa	Low interference	Required difficult two-side deep etching and intricate two-side processing	n/a	n/a	n/a
		Low TS-Extension coupling	Unsuitable for some platforms including flow injection system			
		Large array size and density	Some remaining frequency mode coupling particularly TS-TF			
	Bi-inverted-mesa	Low interference	Required difficult two-side deep etching and intricate two-side processing	High frequency inverted mesa MQCM structure [39,80]	20–94	n/a
		Low TS–extension coupling	Unsuitable for some platforms including flow injection system			
		High resonance frequency, array size and density, mass sensitivity	Some remaining frequency mode coupling particularly TS–TF			

Table 1 (*Continued*)

MQCM structure		Advantages	Disadvantages	Available reported parameters (up to November 2010)		
				References	f_0 (MHz)	Array size
Convex	Plano-convex	Low interference	Required sophisticated patterning and difficult deep etching process	ACR type MQCM for photocatalytic measurement [81]	17	2
		Very Low mode couplings except TS–extension	Limited resonance frequency, mass sensitivity and electrode size			
		Large array size and density	Remaining TS- extension mode coupling			
	Bi-convex	Low interference	Required sophisticated patterning, difficult deep etching process and intricate two-side processing	Fabrication of high Q biconvex MQCM [47]	16	2
		Very Low mode couplings	Unsuitable for some platforms including flow injection system			
		Large array size and density	Limited resonance frequency, mass sensitivity and electrode size			
x-Axis inversion		Low interference	Limited resonance frequency, mass sensitivity and electrode size	Fabrication of *x*-axis inversion by laser process [65]	5	2–6
		Large array size and density No mechanical etching process	Required sophisticated thermal treatment process	LFE type MQCM with *x*-axis inversion [82]	5	2

mination. Examples of receptors in this system are ligands for metal ions [84,85]. For instance, a QCM system with four different ligands having different affinity towards four metal ions can be used to determine the concentrations of the four metal ions [38].

Lastly, an array of different receptors having wide sensitivities towards various components is used to recognize the whole mixture. In this case, components in the mixture and their individual concentrations are not resolved. Most receptors found in nature fall within this category. These include gas-sensitive polymeric and organic materials, electrochemical electrode materials and biochemical enzymes. The QCM array with these receptors gives a pattern of resonance frequency shifts resulting from different receptors' sensitivities towards various ingredients in the composite, which can be analyzed based on pattern recognition methods. Commonly used pattern recognition methodologies are principal component analysis (PCA) [86–92], linear discriminant analysis (LDA) [87,93,94] and neural network [90–92,95]. The main applications for this scheme are odor sensor or electronic nose and taste sensor or electronic tongue.

4.2. Series MQCM as a multichannel detector in the flow injection analysis

A series of identical QCMs with different receptors can alternatively be applied to flow injection analysis for real-time detections as illustrated in Fig. 7. There are some important considerations when MQCM is operated in a flow injection system. Firstly, the structure of MQCM surface in contact with fluid flow should be planar and smooth so that the solution flow will not be disturbed. Thus, MQCM structures with non-smooth surfaces including bi-mesa, bi-inverted-mesa and bi-convex may not be suitable for flow injection analysis [38].

Secondly, analyte should be uniformly dispersed throughout the flow chamber so that all QCMs see the same sample concentration. The effect of flow chamber geometry and flow parameters on sample dispersion in flow injection system with integrated MQCM device has recently been studied by fluid dynamic simulations and flow injection experiments [70]. It has been demonstrated by simulation that MQCM with circular chamber design suffers from non-uniform sample distribution due to turbulent effect while such problem does not occur to MQCM chamber with rectangular design [96]. The results agree to experimental observation that there is a significant variation in resonance frequency shift responses of identical QCMs located in the circular chamber.

A flow injection system containing inverted-mesa MQCM in 20 mm × 20 mm × 0.7 mm square chamber has been demonstrated [7]. The influence of flow rate on uniformity of analyte distribution and the resonant characteristics of QCM is also studied. It is found that the flow rate considerably affects the resonant behaviors of QCM. In addition, spurious oscillation modes are found under low and high flow rate conditions and undesired oscillation can be minimized at an optimum flow rate of 500 μL s^{-1}. Thus, flow rate is another important parameter that must be optimized when MQCM operates in a flow injection system.

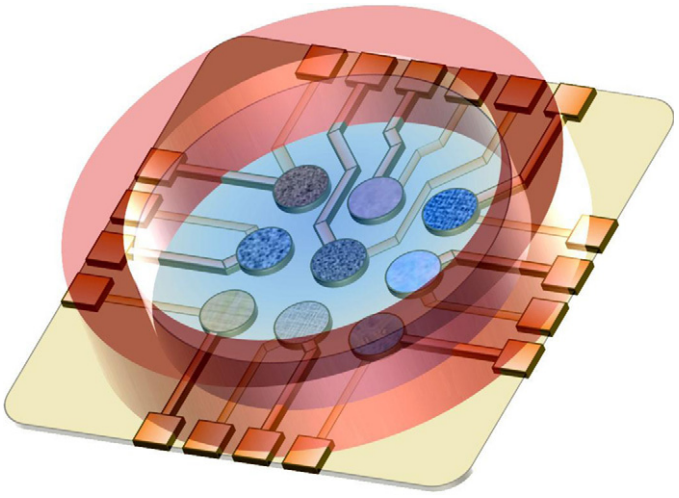

Fig. 6. MQCM platform: a static multichannel detector [38].

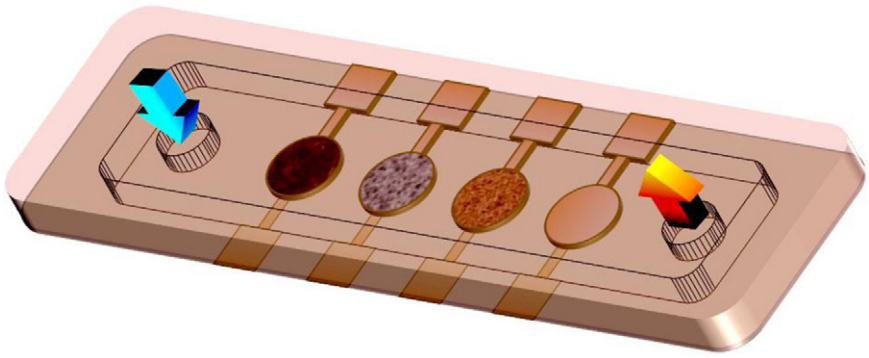

Fig. 7. MQCM platform: a series multichannel detector in flow injection analysis [38].

4.3. Multifrequency QCM as a multi-sensitivity and multi-dynamic range detector

Various QCMs in MQCM can be designed to operate at different resonance frequencies. This platform is termed *multi-frequency QCM* (*MF-QCM*). MF-QCM is typically based on inverted-mesa structures with different mesa thicknesses as illustrated in Fig. 8(a). This structure can be formed by standard mesa micromachining process with additional patterning and etching steps. By this scheme, resonance frequency, mass sensitivity and dynamic range of QCMs can be varied over a wide range of magnitude. A MF-QCM containing an array of 2 mm circular QCM diaphragms with different quartz thicknesses ranging from 77 to 81 μm and corresponding resonance frequencies ranging from 21.7 to 20.75 MHz has been demonstrated [75]. With decreasing quartz thickness, the resonance frequency and mass sensitivity simultaneously increases while the dynamic range decreases. Thus, MF-QCM can provide multi-sensitivity and multi-dynamic-range functionalities [7,38], which is highly valuable for general applications whose sample concentration and detection range are unknown. For multisensitivity and multidynamic range purpose, all QCMs may be modified by only one kind of receptor and the analyte can be detected with high sensitivity and wide dynamic range in one experiment if MF-QCM is properly designed. The multisensitivity and multidynamic range QCM is useful for a wide variety of applications including chemical sensing, bio-sensing and monitoring of surface processes including electrochemical reactions. Moreover, QCMs in an array may be modified with different receptors for multi-component analysis with multi-sensitivity and/or multi-dynamic range capability.

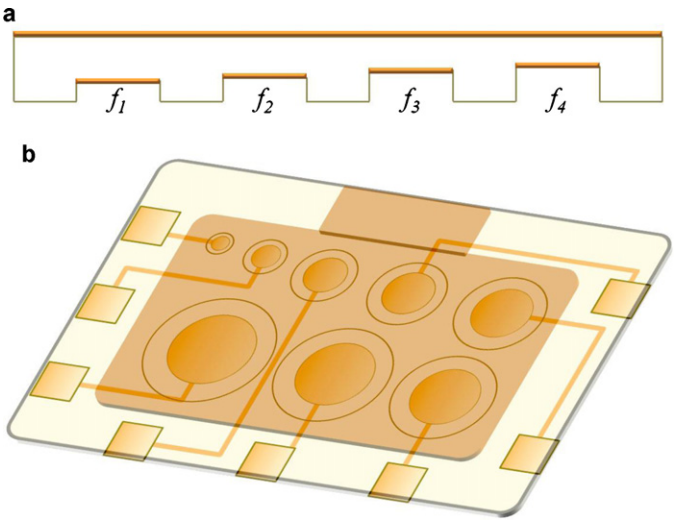

Fig. 8. MQCM platform: a multi sensitivity and dynamic range detector based on (a) varying quartz thickness and (b) varying electrode area [38].

In addition, MF-QCMs may be designed with different electrode sizes as shown in Fig. 8 (b) to further vary mass-sensitivity of QCM array. From Sauerbrey equation (Eq. (1)), the mass sensitivity ($\Delta F/\Delta M$) is inversely proportional to the electrode area (A) and hence mass sensitivity can be significantly increased by decreasing electrode area. Moreover, electrode size also causes small changes to resonance frequency and dynamic range, which cannot be seen from 1D theory. The dependence of resonance frequency on electrode size has been theoretically predicted from 3D finite element simulation [40]. From the simulation, it has been shown that the resonance frequency of QCM decreases as electrode size increases. In addition, the resonance frequency becomes less dependent on diameter for very large diameter values and it will eventually reach the frequency value of 1D theory given in Eq. (2), in which the electrode width is assumed to be infinite. Thus, the variation of electrode size can change the mass-sensitivity with small effects on other design parameters.

5. Potential and prospective applications for MQCM

The advancement of MQCM technology has enabled useful expansion of numerous sensing and measurement techniques based on QCM. Main advantages of MQCM in sensing fields include real-time multi-analyte label-free detection, multi-sensitivity-range sensing and environmental compensation capabilities. In addition, it is potential for real world applications because it can easily made portable. Nevertheless, its applications are still hindered by system/response complexity as well as high cost due to fabrication difficulty. This section presents potential and emerging MQCM applications, which comprise MQCM based gas sensor array as odor sensor or electronic nose, MQCM based chemical sensor array as electronic tongue, MQCM based biosensor array and other miscellaneous applications.

5.1. Odor sensor or electronic nose

Odor sensor or electronic nose is a device that can recognize several odors or gas mixtures. It typically consists of an array of gas sensors having different selectivities and the responses are analyzed by a suitable pattern recognition algorithm. When QCM is employed, gas sensor considerably differs from chemical and biosensors due to great differences of viscoelastic properties of sensing film and analyte. The characteristics of QCM based gas sensor are mainly determined by viscoelastic properties of sensing film while gas phase analyte only modifies the mass per unit area. Thus, QCM based gas sensor can easily be analyzed and developed. MQCM based odor sensor represents the first and the most

successful application of MQCM based sensor. QCMs in MQCM platform are selectively deposited with different gas-sensitive layers. Most gas-sensing materials employed in MQCM are organic and polymeric materials, which can physically adsorb gases at room temperature. Several gas sensor arrays based on conventional MQCM structure have been reported [71]. For example, a 10 MHz MQCM selectively coated with three sensing films including ionic liquid butylmethylimidazolium camphorsulfonate (BMICS), ionic liquid butylmethylimidazolium tetrafluoroborate ($BMIBF_4$) and poly(vinyl ferrocene) (PVF) by solvent casting are developed for classification and detection of humidity (water vapor) and volatile organic compounds (VOCs) including ethanol, dichloromethane (CH_2Cl_2) and hexane. The study results show that the sensors with different coatings exhibit different frequency shift characteristics towards various analytes. For example, BMICS is highly sensitive to ethanol while PVF is more sensitive to CH_2Cl_2. From the sensing patterns, VOCs and humidity can be well discriminated by the sensor array with LDA analysis.

Another interesting instance is a 10 MHz QCM gas sensor array coated with Poly-vinyl-pyrrolidon (PPy) and DM-189 organic precursor material for humidity and ammonia sensing [66]. A remarkable feature of this QCM array is that it has integrated heater for gas sensing in temperature modulation (TM) mode. In TM mode, gas adsorption on QCM is purged by rapid heating over a short period and gas sensing response is obtained from the frequency difference between gas-sensing and gas-purging periods. The advantages of this scheme are fast recovery and possible elimination of reference QCM. However, it requires additional heater and can suffers from short life time due to rapid heating and cooling. Moreover, the magnitude of resonance frequency shift from conventional MQCM gas sensor array is only on the order of hundreds of Hertz, which is considered small and not sufficient for many applications involving much lower vapor concentration.

Several strategies have been employed to enhance sensitivity of MQCM gas sensor array. Firstly, MQCM can be designed to operate at high resonance frequency in order to increase mass-sensitivity for gas molecule detection. This scheme is very effective because the resonance frequency shift is proportional to the square of resonance frequency. For instance, an odor sensor based on MQCM utilizing plano-inverted-mesa structure has been demonstrated [75]. QCMs are designed to operate a high frequency of ~21 MHz and are coated with three amphiphilic organic materials, including dimyristylphosphatidylchorine (DMPC), dimyristylphosphatidylserine (DMPS) and cholesterol by solvent casting. It has shown high sensitivity and ability to discriminate six kinds of odorants including ethanol, methanol, benzene, methyl-benzene, CH_2Cl_2 and CH_3COCH_3.

Another important strategy is to use highly sensitive gas-sensing films based on nanostructured materials. A wide variety of nanomaterials have been applied to QCM gas sensor array [97,98]. Following highlights some interesting examples of nanostructure materials integrated on QCM gas sensor arrays. Mesoporous silica hybrids are interesting nanostructure materials, which have successfully been applied to QCM gas sensor array. Conventional MQCM are coated with unmodified mesoporous silica and mesoporous silica hybridized with β-cyclodextrin (β-CD) and triphenylphosphine (PPh3) for alcohol and benzene discrimination [67]. The results show that nanohybrid structures provide enhanced sensitivity while β-CD and PPh3-silica composites are very effective for discrimination between benzene and alcochol.

Carbon nanotubes (CNTs) are one of the most widely studied nanomaterials with promising properties for gas-sensing [99–102]. They have been applied to several QCM and MQCM gas sensing platforms. An interesting example of CNTs applications is the use of isolated single walled (SW) CNTs on QCM sensor array for highly sensitive detection of small gas molecules including helium, nitrogen, oxygen, argon and sulfurhexafluoride (SF_6) [76]. The MQCM has plano-inverted-mesa structure with mesa thickness of ~56 μm and SW-CNTs are coated on gold electrodes by spray coating of SW-CNTs in NMP (N-methyl-2-pyrrolidinone). It has been demonstrated that SW-CNTs provide highly sensitive detection of small gas molecules with large frequency and *Q*-factor changes and they are logarithmically proportional to the mass of gas molecules. *Q*-factor change is attributed to viscoelastic dissipation of non-rigidly adsorbed gas molecules around CNT walls.

Molecularly imprinted polymer (MIP) is a class of nanostructured organic materials, which can be designed as analyte receptors with various specificities [2,103]. MIPs are synthesized by polymerization of monomers in the presence of analytes acting as templates, which are subsequently removed by evaporation leaving cavities within the polymer matrix. Different analytes will distinctively bind to molecular cavities, resulting in desired selectivities. This approach can be used to sensitively distinguish similar isomers with sufficient selectivity. MIPs have been applied to MQCM to sense a group of terpenes, which are biogenic volatile compounds emanating from herbaceous vegetation [74]. Six MIPs are synthesized from six terpenes templates including α-pinene, limonene, eucalyptol, β-pinene, terpinene and estragole with polystyrene (PS) and divinylbenzene (DVB) copolymer matrix. MIPs are synthesized by mixing terpene templates to styrene functional monomer, DVB cross-linker, AIBN radical initiator and diphenylmethane. The mixtures are polymerized for 40 min at 70 °C and then selectively deposited on electrodes by spin coating with photoresist patterning. It has been shown that each analyte shows maximum selectivity towards its corresponding template. In addition, it shows selectivity between isomeric compounds, α-pinene and β-pinene. These selectivity patterns are successfully analyzed by a neural network methodology.

MQCM based e-noses have recently been demonstrated in real-world applications. For instance, MQCM based enose has been used for plant-degradation monitoring [104]. MQCM comprises six QCM electrode coated with six different polymer and MIP layers that can distinctively detect humidity, alcohol, ester and terpene compounds. It has been used to monitor VOCs emitted from grass and pine composting processes. The e-nose system has successfully provided real time data of VOCs compositions, which have been validated by gas chromatography mass-spectrometry (GC–MS) and given direct insight into the differences between grass and pine composting batches, which are beneficial for composting process control. This demonstrates that MQCM based e-noses should be potential for other real world applications such as environmental monitoring, industrial/agricultural gas monitoring, food/drink quality control, detection of emitted diseases, etc. Nevertheless, more experimental work needs to be done to realize these target applications.

5.2. Chemical sensor array

Chemical sensor array and electronic tongue are devices for multiple detection of chemical and chemical compound. In chemical sensor array, QCMs are coated with different chemical receptors, which absorbed analyte, resulting in negative resonance frequency shift. In general, chemical receptors are not specific and several chemical receptors are normally used to identify and quantify an analyte. For instance, flow injection MF-QCM for detection of toluene has been reported [7]. In this system, three organic materials including polystyrene, amyl-calix [8] arene and β-cyclodextrine are used as toluene receptors. The receptors are coated using electrostatic spray or airbrush techniques. Resonance frequency and equivalent resistance of QCMs are monitored during flow injection of toluene in water stream. It is found that polystyrene and amyl-calix [8] arene give similar response while β-cyclodextrine

exhibits an unusual response. For the first two sensors, the resonance frequencies decrease whereas the equivalent resistances increase upon toluene injection. The frequency decrease is due to mass accumulation caused by the penetration of toluene into the coating while the increased resistance indicates that acoustic dissipation decreases due to the reduced shear modulus of the surface. However, the frequency shift is relatively lower whereas the resistance increase is much larger and response is notably faster for QCM coated with amyl-calix [8] arene. For β-cyclodextrine case, the frequency temporarily increases and decreases while equivalent resistance decreases strongly and steadily upon toluene and water injections. This indicates that toluene is not rigidly absorbed into β-cyclodextrine unlike other coating cases. The difference in response of QCMs with different coating can be used to uniquely identify and determine the concentration of analyte. However, it is known that the responses in liquid are considerably more complicated than those in gas phase. The behaviors of QCM based chemical sensor are more complex due to contribution by viscoelastic properties of both sensing film and solution. In addition, liquid-film interaction such as swelling can further complicate the sensing response. Thus, the analysis of response requires sophisticated methods that may require human intervention and there is no standard formulation and method for this purpose. Presently, there has been no report of MQCM based electronic tongue due to complicated response and interference in liquid. Owing to its wide real world applications such as food, drink and medicine analysis, MQCM based electronic tongue is a challenging topic that is currently under exploration.

5.3. Biosensor array

Research on QCM for biosensor has grown steadily by increasing health care, agricultural and security needs. Various classes of QCM biosensors including immune [27,105–107], enzyme [108,109], nucleic acid [83,110,111] and cell [112,113] based sensors have been presented. Biosensor arrays based on simple combination of QCMs have also been developed for multiple and simultaneous detection of bioanalytes of the same or different classes [114,115]. However, this scheme requires large sample consumption and environmental control among different sensors is difficult. MQCM technology is thus a key to realize efficient miniaturized biosensor array. MQCM Biosensor array can be achieved by the selective application of different functional bioreceptors atop various QCM elements to provide molecular hooks or active sites for a range of analytes of interest. In addition, multi-sensitivity and multi-dynamic-range QCM platforms allow simultaneous detections of biological species of different sizes ranging from virus, DNA, protein to complex arrays of biomacromolecules and large cells on one chip.

Functionalization of biological receptors on QCM's gold electrodes are most commonly done by the use of self-assembled monolayer (SAM) techniques. SAMs of alkanethiols are typically formed on gold by adsorption from dilute solutions [116–119]. The general structure of alkanethiols is $HS(CH_2)nX$, where n is an integer and typically varies between 14 and 16 in. long chain molecules, and X is terminal group in a series including $-CH_3$, $-CH_2OH$, $-CO_2H$, $-CO_2CH_3$, $-CONH_2$ and more complex functional groups [77]. The thiol group (SH) binds spontaneously to gold with a relatively strong binding energy approximately of 120 kJ mol^{-1}, producing very stable and uniform layer. Terminal groups of SAMs are selected to provide match binding to target species or their biological receptors.

Recently, a fair number of studies on MQCM based biosensor arrays have been reported [72,77,79]. However, most reports have only demonstrated functionalizations of a few distinct biological receptors on one chip and detection of a few biological analytes. For instance, 8-pixel QCM array for bovine serum albumin (BSA) and avidin detections have been reported [79]. Some pixels are selectively functionalized with 3,3′-dithiobis (sulfosuccinimidylpropionate) (DTSSP) for avidin detection while others are masked using photoresist and octadecanethiol (ODT) SAMs are subsequently functionalized for BSA detection. The resonance frequency shifts of 460 and 76 Hz are obtained from selectively functionalized QCMs for 10 mg mL^{-1} BSA and 1 mg mL^{-1} avidin, respectively.

A MQCM based biosensor has also been reported for yeast cell detection utilizing MIP methodology [72]. Yeast-sensitive receptors are generated by molecular imprinting of single and duplex yeast cells in polyurethane films. Synthetic *Saccharomyces cerevisiae* yeast cells is blended with 4,4′-diisocyanato diphenylmethane, bisphenol and phloroglucinol prepolymer mixture at 70 °C and spun on conventional 10 MHz MQCM electrodes. The mixture is then polymerized over night and yeast templates are removed by ultrasonication in water. Yeast cells are detected by flow injection analysis and flow injection response to a single yeast cell solution of MQCM with four different MIP coated electrodes. It is demonstrated that MIP imprinted with single and duplex cells has strong response to their respective yeast cells while two non-imprinted electrodes and the one imprinted with different cell type give only a minor frequency decrease. Thus, MIP layers exhibit very good selectivity for yeast cell detection.

There have been several efforts to develop MQCM based immunosensors, which immobilized several antibodies for detection of various species. Nevertheless, no study succeeded in establishing the MQCM based immunosensors because of intricate QCM sensing response and ineluctable interference among channels operating in real biological solutions [120]. QCM based biosensor's responses are more intricate than that of chemical sensor due to the complex nature of biological receptors and analytes. In addition, biological samples such as antigen-antibody and cells are often formed heterogeneously on electrode surface, making response analysis even more complicated. Thus, a lot more work on MQCM based biosensors including selective functionalization of micro-QCM array, inference reduction, advanced analysis and characterizations of multiple biosensing in real environment need to be done to realize effective biosensor arrays for real world applications including clinical diagnosis, agricultural, horticultural, veterinary and microbial contamination analyses and other biomedical applications.

5.4. Miscellaneous applications

In addition to gas, chemical and biosensor arrays, several specific and special applications for MQCM have been proposed. Photocatalytic reaction measurement is a new potential application for QCM [121,122]. Photocatalytic materials have attracted great attention due to their ability to decompose organic pollutants under near UV irradiation and photocatalytic activity has normally been measured by monitoring the color degradation of dyes on photocatalytic materials [123]. It is desirable to study photocatalytic effect without addition of dye molecules. QCM can be used to measure the mass change effects caused by photocatalytic reactions with no dye molecule. However, QCM is sensitive to decomposition reaction's conditions including UV radiation intensity and temperature and such dependence must be effectively compensated. Recently, dual QCM scheme based on antiparallel coupled resonator (ACR) structure (ACR is a new type of thickness field excited QCM, which has two electrodes one side of AT-cut quartz and a conducting layer on the other side [73]) has successfully been applied for photocatalytic activity of methylene blue (MB) measurement [81]. It has been demonstrated that the environmental effects induced by UV irradiation and gradual temperature changes can be well compensated by the referenced QCM on the same quartz substrate. In addition,

Table 2
Summary of MQCM platforms and applications.

MQCM platforms	Reported structures	Application areas	Potential applications	Reported applications
Static multichannel detector	Conventional QCM Plano-inverted-mesa QCM	Multi-component analysis with selective receptors Multi-component analysis with low selectivity receptors for quantification of component Multi-component analysis with low selectivity receptors for mixture recognition	Electronic noses Chemical sensor array Electronic tongues Biosensor array Multi-photocatalytic measurement Multi-EQCM	Electronic noses: VCO and humidity detection [66,67,71,74–76,104] Biosensor array: Avidine and BSA detection [79]
Series MQCM as a multichannel detector for the flow injection analysis	Conventional QCM Plano-inverted-mesa QCM	High throughput multi-component analysis		Chemical sensor array: toluene detection [7] Biosensor array: yeast cell detection [72]
Multifrequency QCM for multi-sensitivity and multi-dynamic range detection	Plano-inverted-mesa QCM	Multi-sensitivity detection Multi-dynamic range detection Multi-component analysis		Chemical sensor array: Toluene [7]

the resulting frequency shift versus irradiation intensity of UV light exhibits a linear relationship, making MQCM highly practical for this application. This scheme should be extended to multiple simultaneous activity measurements of several photocatalytic materials.

A large number of applications in the field of electroanalytical chemistry of single EQCM have been reported [124,125]. These include studies of formation, viscoelastic behavior, and ion/solute transport properties of electropolymerized films. For example, EQCM has been used to monitor the electropolymerization of polypyrrole and to investigate the film evolution from elastic behavior early in the polymerization process to visoelastic, energy dissipating properties in the subsequent synthesis of a thicker film. The details of ion and solvent transport between the film and solution can be sensitively followed through mass change related to concentration changes in any small diffusing species that migrate in the film. The diverse applicability should be extended to multiple EQCMs based on MQCM structure so that multiple studies can be simultaneously performed. However, there has been no report of multi-EQCMs based on MQCM structure. In EQCM array systems, channels of MQCM can be used as different working electrodes operating at distinct applied potentials and one of channel may be used as a counter electrode. However, strong electric and acoustic interference and other problems in multi-EQCM system are still major barriers for the development. Therefore, multi-EQCMs based on MQCM platform are one of challenging topics that should be further explored.

Table 2 summarizes the MQCM platforms, reported structures, application areas, potential and reported applications and Table 3 lists sensing materials, target analytes, sensitivity and sensing range of reported MQCM based sensors. It can be seen that only conventional MQCM and plano-inverted-mesa MQCM structures have been applied to various MQCM platforms. This should be due to the fact that conventional MQCM can be most easily implemented while plano-inverted-mesa structure provides numerous advantages in terms of interference, resonance frequency and mass sensitivity and it is applicable to flow injection and multi-frequency/multi-dynamic-range platforms. Moreover, it can be seen that among implemented MQCM potential applications, only electronic noses have been most successfully demonstrated in laboratories as well as real world applications while chemical/biosensor arrays have only been demonstrated to a few examples of analytes. From Table 3, sensing materials are mostly organics or polymer, which sometimes hybrid with inorganic nanomaterials, while only limited groups of target analytes have been studied over some

Table 3
Summary of sensing parameters of reported MQCM based sensors (up to September 2010).

MQCM application	Sensing materials	Target analytes	Sensitivity	Sensing range	Ref.
Electronic noses	CPH, DM 189, PPy	Ammonia, humidity	~1, ~0.1 Hz ppm^{-1}	0-1000, 0-20000 ppm	[66]
	β-CD-, PPh_3-Meso silica	Benzene, alcohol	0.05-0.09, 0.01-0.02 Hz ppm^{-1}	0-5000 ppm	[67]
	BMICS, BMIBF4, PVF	Ethanol, CH_2Cl_2, hexane, humidity	0.2-1, 2-6, 0.1-1, 0.1-0.5 Hz %$^{-1}$	10%	[71]
	MIP: α-Pinene, β-Pinene Limonene, Terpinene, Estragole, Eucalyptol	α-Pinene, β-pinene, limonene, terpinene, estragole, eucalyptol	n/a	n/a	[74]
	DMPC, DMPS, cholesterol	Ethanol, methanol, benzene, methyl-benzene, CH_2Cl_2, CH_3COCH_3	n/a	n/a	[75]
	PVA, PS, PU, MIP:PS/DVB	Alcohol, limonene, ethyl acetate, humidity	n/a	0–300 ppm	[104]
	SW-CNTs-NMP	Helium, nitrogen, oxygen, argon, SF_6	50–100 Hz amu^{-1}	4–100 amu	[76]
Chemical sensor array	PS, amyl-calix[8]arene, β-CD	Toluene	10–100 Hz ppm^{-1}	400 ppm	[7]
Biosensor array	DTSSP, ODT	Avidine, BSA	30–70 Hz (mg mL)$^{-1}$	0–1 mg mL^{-1}	[79]
	MIP: yeast cell	Yeast cell	~1 cell mL^{-1}	5×10^5 cell μL^{-1}	[72]

CPH: cryptophane, PPy: β-CD:β-cyclodextrine, PPh_3: triphenylphosphine, BMICS: ionic-liquid-butylmethylimidazolium-camphorsulfonate, BMIBF4: ionic-liquid butylmethylimidazolium-tetrafluoroborate, PVF: polyvinyl-ferrocene, DMPC: dimyristylphosphatidylchorine, DMPS: dimyristylphosphatidylserine, PVA: polyvinyl-alcohol, PS: polystyrene, PU: polyurethane, MIP: molecularly imprinted polymer, DVB: divinylbenzene, SW-CNTs-NMP, DTSSP: 3,3′-dithiobis (sulfosuccinimidylpropionate), ODT: octadecanethiol, BSA: bovine serum albumin, amu: atomic mass unit.

reported sensing ranges and sensitivities. Furthermore, electronic tongue, multi-biosensor and multi-EQCM have not yet been developed. Therefore, most MQCM based sensors require much further development before they can be routinely used in laboratories and real world applications.

6. Conclusion

In conclusion, MQCM technology has been extensively reviewed. The theoretical/experimental analysis, design, acoustic interference and other problems of conventional MQCM's have been discussed. Various MQCM schemes devices based on modification of quartz substrate structure including mesa, convex and *x*-axis inversion structures are then presented. Among these, plano-inverted-mesa has been the most frequently reported because it simultaneously offers low interference, high resonance frequency, high mass sensitivity and compatibility with flow injection and multi-frequency system. Next, MQCM sensing platforms comprising static multichannel detector, series MQCM as a multichannel detector for the flow injection analysis, multi-frequency QCM for multi-sensitivity/multi-dynamic range detection are described. The combination of multi-frequency QCM and flow injection analysis platforms are seen to be most promising for various application areas. Lastly, potential and prospective MQCM applications are illustrated. Electronic noses is found to be the most successful application with real world demonstration while electronic tongue, biosensor array and other applications are still at an early stage of development. Therefore, MQCM is a relatively new and promising research area worthy for further exploration.

Acknowledgement

This work is supported by National Electronics and Computer Technology Center (NECTEC) under QCM biosensor project and Thailand Research Fund (TRF). A.T. would like to acknowledge TRF for career developing fund.

References

[1] K.A. Marx, Biomacromolecules 4 (2003) 1099–1120.
[2] B. Wyszynski, T. Nakamoto, IEEJ Trans. Elec. Electron. Eng. 4 (2009) 334–338.
[3] J.F. Alder, J.J. McCallum, Analyst 108 (1983) 1169–1189.
[4] Y. Uludag, S.A. Piletsky, A.P.F. Turner, M.A. Cooper, FEBS J. 274 (2007) 5471–5480.
[5] X. Su, F.T. Chew, S.F.Y. Li, Anal. Sci. 16 (2000) 107–114.
[6] K.D. Pavey, Expert Rev. Mol. Diagn. 2 (2002) 173–186.
[7] J. Rabe, S. Büttgenbach, J. Schröder, P. Hauptmann, IEEE Sens. J. 3 (2003) 361–368.
[8] G. Sauerbrey, Z. Phys. 155 (1959) 206–222.
[9] K. Keiji Kanazawa, J.G. Gordon Ii, Anal. Chim. Acta 175 (1985) 99–105.
[10] M.D. Ward, E.J. Delawski, Anal. Chem. 63 (1991) 886–890.
[11] Z. Lin, C.M. Yip, I. Scott Joseph, M.D. Ward, Anal. Chem. 65 (1993) 1546–1551.
[12] M. Rodahl, B. Kasemo, Sens. Actuators B 37 (1996) 111–116.
[13] H. Muramatsu, E. Tamiya, I. Karube, Anal. Chem. 60 (1988) 2142–2146.
[14] M. Rodahl, F. Höök, C. Fredriksson, C.A. Keller, A. Krozer, P. Brzezinski, M. Voinova, B. Kasemo, Faraday Discuss. 107 (1997) 229–246.
[15] M. Penza, G. Cassano, P. Aversa, F. Antolini, A. Cusano, A. Cutolo, M. Giordano, L. Nicolais, Appl. Phys. Lett. 85 (2004) 2379–2381.
[16] M. Matsuguchi, T. Uno, Sens. Actuators B 113 (2006) 94–99.
[17] L.C. Brousseau Iii, T.E. Mallouk, Anal. Chem. 69 (1997) 679–687.
[18] B. Ding, J. Kim, Y. Miyazaki, S. Shiratori, Sens. Actuators B 101 (2004) 373–380.
[19] X. Wang, J. Zhang, Z. Zhu, Appl. Surf. Sci. 252 (2006) 2404–2411.
[20] M.D. Ward, in: I. Rubenstein (Ed.), Physical Electrochemistry: Principles Methods & Applications, Marcel Dekker, New York, 1995.
[21] N. Asakura, T. Kamachi, I. Okura, Res. Chem. Intermed. 32 (2006) 341–355.
[22] M. Lukaszewski, A. Czerwhiski, J. Electroanal. Chem. 606 (2007) 117–133.
[23] C.K. O'Sullivan, G.G. Guilbault, Biosens. Bioelectron. 14 (1999) 663–670.
[24] A. Janshoff, H.J. Galla, C. Steinem, Angew. Chem. Int. Ed. 39 (2000) 4004–4032.
[25] J. Wegener, A. Janshoff, L. Steinem, Cell Biochem. Biophys. 34 (2001) 121–151.
[26] B.A. Čavić, G.L. Hayward, M. Thompson, Analyst 124 (1999) 1405–1420.
[27] F. Ricci, G. Volpe, L. Micheli, G. Palleschi, Anal. Chim. Acta 605 (2007) 111–129.
[28] P.D. Skottrup, M. Nicolaisen, A.F. Justesen, Biosens. Bioelectron. 24 (2008) 339–348.
[29] E.R. Hirst, Y.J. Yuan, W.L. Xu, J.E. Bronlund, Biosens. Bioelectron. 23 (2008) 1759–1768.
[30] T.S. Hug, Assay Drug Dev. Technol. 1 (2003) 479–488.
[31] V.E. Bottom, Introduction to Quartz Crystal Unit Design, Van Nostrand Reinhold, New York, 1982.
[32] S. Bruckenstein, A. Fensore, Z. Li, A.R. Hillman, J. Electroanal. Chem. 370 (1994) 189–195.
[33] S. Bruckenstein, M. Michalskl, A. Fensore, L.I. Zhufen, A.R. Hillman, Anal. Chem. 66 (1994) 1847–1852.
[34] G.C. Dunham, N.H. Benson, D. Petelenz, J. Janata, Anal. Chem. 67 (1995) 267–272.
[35] T. Uno, Frequency Control Symposium, 1996, in: 50th, Proceedings of the 1996 IEEE International, 1996, pp. 526–531.
[36] S. Berg, D. Johannsmann, Anal. Chem. 73 (2001) 1140–1145.
[37] F. Shen, K.H. Lee, S.J. O'Shea, P. Lu, T.Y. Ng, IEEE Sens. J. 3 (2003) 274–281.
[38] T. Tatsuma, Y. Watanabe, N. Oyama, K. Kitakizaki, M. Haba, Anal. Chem. 71 (1999) 3632–3636.
[39] V.N. Hung, T. Abe, P.N. Minh, M. Esashi, Appl. Phys. Lett. 81 (2002) 5069–5071.
[40] F. Lu, H.P. Lee, P. Lu, S.P. Lim, Sens. Actuators A 119 (2005) 90–99.
[41] S.J. Martin, V.E. Granstaff, G.C. Frye, Anal. Chem. 63 (1991) 2272–2281.
[42] R.W. Cernosek, S.J. Martin, A.R. Hillman, H.L. Bandey, IEEE Trans. Ultrason. Ferroelectr. Freq. Control 45 (1998) 1399–1407.
[43] H.F. Tiersten, Linear Piezoelectric Plate Vibrations, Plenum, New York, 1969.
[44] F. Shen, P. Lu, IEEE Trans. Ultrason. Ferroelectr. Freq. Control 51 (2004) 249–253.
[45] R.D. Mindlin, P.C.Y. Lee, Int. J. Solids Struct. 2 (1966) 125–139.
[46] Y.-K. Yong, J.T. Stewart, J. Detaint, A. Zarka, B. Capelle, Y. Zheng, IEEE Trans. Ultrason. Ferroelectr. Freq. Control 39 (1992) 609–617.
[47] L. Li, T. Abe, M. Esashi, Proceedings of the IEEE International Conference on Micro Electro Mechanical Systems (MEMS) (2005) 327–330.
[48] A. Ishizaki, H. Sekimoto, D. Tajima, Y. Watanabe, Proceedings of the IEEE Ultrasonics Symposium 2 (1995), 913–916.
[49] S. Goka, H. Sekimoto, Y. Watanabe, Proceedings of the Annual IEEE International Frequency Control Symposium 1 (1999) 441–444.
[50] K. Hirama, Y. Aoyama, M. Naito, Jpn. J. Appl. Phys., Part 1 36 (1997) 6432–6436.
[51] K.M. Lakin, G.R. Kline, K.T. McCarron, Proceedings of the Annual IEEE International Frequency Control Symposium, (1995), 827–831.
[52] H. Sekimoto, S. Goka, Y. Watanabe, IEEE Trans. Ultrason. Ferroelectr. Freq. Control 48 (2001) 1302–1307.
[53] C. Kreutz, J. Lörgen, B. Graewe, J. Bargon, M. Yoshida, Z.M. Fresco, J.M.J. Frèchet, Sensors 6 (2006) 335–340.
[54] S. Goka, H. Sekimoto, Y. Watanabe, Proceedings of the Annual IEEE International Frequency Control Symposium, (2000) 397–400.
[55] H. Iwata, IEEE Trans. Ultrason. Ferroelectr. Freq. Control 51 (2004) 1026–1029.
[56] H. Iwata, IEEE Trans. Ultrason. Ferroelectr. Freq. Control 52 (2005) 1435–1442.
[57] F. Shen, S.J. O'Shea, K.H. Lee, P. Lu, T.Y. Ng, IEEE Trans. Ultrason. Ferroelectr. Freq. Control 50 (2003) 668–675.
[58] F. Shen, P. Lu, S.J. O'Shea, K.H. Lee, Sens. Actuators A 111 (2004) 180–187.
[59] S. Goka, K. Tamura, H. Sekimoto, Y. Watanabe, T. Sato, Proceedings of the Annual IEEE International Frequency Control Symposium, (2003) 694–697.
[60] Y. Nagaura, K. Kinoshita, S. Yokomizo, Frequency Control Symposium and Exhibition, 2000, in: Proceedings of the 2000 IEEE/EIA International, 2000, pp. 255–259.
[61] L. Li, T. Abe, M. Esashi, Sens. Actuators A 114 (2004) 496–500.
[62] Z. Nagaura, K. Nagaura, K. Imani, Y. Nagaura, Frequency Control Symposium and Exposition, 2005, in: Proceedings of the 2005 IEEE International, 2005, pp. 588–593.
[63] S. Noge, E. Kamiyama, Y. Ueoka, T. Uno, Ultrasonics Symposium, 1997, in: Proceedings., 1997 IEEE, 1042, 1997, pp. 1043–1046.
[64] S. Noge, M. Kurita, T. Uno, Ultrasonics Symposium, 1999, in: Proceedings. 1999 IEEE, 631, 1999, pp. 633–636.
[65] S. Noge, T. Uno, Frequency and Time Forum, 1999 and the IEEE International Frequency Control Symposium, 1999, in: Proceedings of the 1999 Joint Meeting of the European, 471, 1999, pp. 477–480.
[66] P. Boeker, G. Horner, S. Rösler, Sens. Actuators B 70 (2000) 37–42.
[67] A. Palaniappan, X.D. Su, F.E.H. Tay, IEEE Sens. J. 6 (2006) 1676–1682.
[68] S. Pantalei, E. Zampetti, A. Macagnano, A. Bearzotti, I. Venditti, M.V. Russo, Sensors 7 (2007) 2920–2928.
[69] E. Zampetti, S. Pantalei, A. Macagnano, E. Proietti, C. Di Natale, A. D'Amico, Sens. Actuators B 131 (2008) 159–166.
[70] K. Jaruwongrungsee, T. Maturos, P. Sritongkum, M. Sangworasil, A. Wisitsoraat, A. Tuantranont, Int. J. Appl. Biomed. Eng. 2 (2009) 50–54.
[71] X.X. Jin, Y. Huang, A. Mason, X.Q. Zeng, Anal. Chem. 81 (2009) 595–603.
[72] K. Seidler, M. Polreichova, P.A. Lieberzeit, F.L. Dickert, Sensors 9 (2009) 8146–8157.
[73] T. Abe, IEEE Sens. J. 11 (2011) 86–90.
[74] N. Iqbal, G. Mustafa, A. Rehman, A. Biedermann, B. Najafi, P.A. Lieberzeit, F.L. Dickert, Sensors 10 (2010) 6361–6376.
[75] T. Abe, M. Esashi, Sens. Actuators A 82 (2000) 139–143.
[76] A. Goyal, P. Joshi, S. Tadigadapa, A. Gupta, P. Eklund, Proceedings of IEEE Sensors (2005) 841–844.
[77] P. Kao, A. Goyal, D. Allara, S. Tadigadapa, TRANSDUCERS and EUROSENSORS '07-4th International Conference on Solid-State Sensors, Actuators and Microsystems (2007) 2311–2314.
[78] S. Winters, G. Bernhardt, D.J. Frankel, J. Vetelino, Proceedings of the IEEE Ultrasonics Symposium (2008) 272–275.

[79] P. Kao, S. Doerner, T. Schneider, D. Allara, P. Hauptmann, S. Tadigadapa, J. Microelectromech. Syst. 18 (2009) 522–530.
[80] V.N. Hung, T. Abe, P.N. Minh, M. Esashi, Sens. Actuators A 108 (2003) 91–96.
[81] T. Abe, H. Kato, J. Micromech. Microeng. 19 (2009) 094019.
[82] M. Wark, S. Winters, C. York, W. Pinkham, G. Bernhardt, J.F. Vetelino, Ultrasonics Symposium, 2006, IEEE (2006) 880–883.
[83] I. Mannelli, M. Minunni, S. Tombelli, M. Mascini, Biosens. Bioelectron. 18 (2003) 129–140.
[84] F. Höök, M. Rodahl, B. Kasemo, P. Brzezinski, Proc. Natl. Acad. Sci. U. S. A. 95 (1998) 12271–12276.
[85] A.M. Etorki, A. Robert Hillman, K.S. Ryder, A. Glidle, Electroanal. J. Chem. 599 (2007) 275–287.
[86] S. Mildner-Szkudlarz, H.H. Jeleń, Food Chem. 110 (2008) 751–761.
[87] A.M. Martinez, A.C. Kak, IEEE T. Pattern. Anal. 23 (2001) 228–233.
[88] A. Pavlou, A.P.F. Turner, N. Magan, Lett. Appl. Microbiol. 35 (2002) 366–369.
[89] P. Boilot, E.L. Hines, M.A. Gongora, R.S. Folland, Sens. Actuators B 88 (2003) 80–88.
[90] A. Branca, P. Simonian, M. Ferrante, E. Novas, R.M. Negri, Sens. Actuators B 92 (2003) 222–227.
[91] R. Dutta, D. Morgan, N. Baker, J.W. Gardner, E.L. Hines, Sens. Actuators B 109 (2005) 355–362.
[92] M. Peris, L. Escuder-Gilabert, Anal. Chim. Acta 638 (2009) 1–15.
[93] L.F. Chen, H.Y.M. Liao, M.T. Ko, J.C. Lin, G.J. Yu, Pattern Recog. 33 (2000) 1713–1726.
[94] T. Hastie, R. Tibshirani, IEEE T. Pattern. Anal. 18 (1996) 607–616.
[95] C. Li, P. Heinemann, R. Sherry, Sens. Actuators B 125 (2007) 301–310.
[96] K. Jaruwongrungsee, T. Maturos, P. Sritongkum, A. Wisitsora-At, C. Pintavirooj, M. Sangworasil, A. Tuantranont, ECTI-CON 2010 – The 2010 ECTI International Conference on Electrical Engineering/Electronics, Computer, Telecommunications and Information Technology (2010) 548–551.
[97] M. Consales, S. Campopiano, A. Cusano, M. Penza, P. Aversa, L. Capodieci, M. Giordano, Proceedings of SPIE – The International Society for Optical Engineering (2005) 46–49.
[98] M. Penza, G. Cassano, P. Aversa, F. Antolini, A. Cusano, M. Consales, M. Giordano, L. Nicolais, Sens. Actuators B 111–112 (2005) 171–180.
[99] L. Valentini, I. Armentano, J.M. Kenny, C. Cantalini, L. Lozzi, S. Santucci, Appl. Phys. Lett. 82 (2003) 961–963.
[100] M. Trojanowicz, TrAC Trends Anal. Chem. 25 (2006) 480–489.
[101] N. Du, H. Zhang, B. Chen, M. Xiangyang, Z. Liu, J. Wu, D. Yang, Adv. Mater. 19 (2007) 1641–1645.
[102] T. Zhang, S. Mubeen, N.V. Myung, M.A. Deshusses, Nanotechnology 19 (2008) 332001.
[103] C. Steinem, A. Janshoff, F.L. Dickert, P.A. Lieberzeit, Piezoelectric Sensors (Springer Series on Chemical Sensors and Biosensors), Springer, Berlin, Heidelberg, 2007, 173–210.
[104] P.A. Lieberzeit, A. Rehman, B. Najafi, F.L. Dickert, Anal. Bioanal. Chem. 391 (2008) 2897–2903.
[105] C.K. O'Sullivan, R. Vaughan, G.G. Guilbault, Anal. Lett. 32 (1999) 2353–2377.
[106] Y.S. Fung, Y.Y. Wong, Anal. Chem. 73 (2001) 5302–5309.
[107] R.D. Vaughan, C.K. O'Sullivan, G.G. Guilbault, Enzyme Microb. Technol. 29 (2001) 635–638.
[108] S.M. Reddy, J.P. Jones, T.J. Lewis, P.M. Vadgama, Anal. Chim. Acta 363 (1998) 203–213.
[109] F. Patolsky, M. Zayats, E. Katz, I. Willner, Anal. Chem. 71 (1999) 3171–3180.
[110] J. Wang, Anal. Chem. 69 (1997) 5200–5202.
[111] F. Patolsky, A. Lichtenstein, I. Willner, J. Am. Chem. Soc. 122 (2000) 418–419.
[112] J. Wegener, A. Janshoff, H.J. Galla, Euro. Biophys. J. 28 (1998) 26–37.
[113] K.A. Marx, T. Zhou, A. Montrone, H. Schulze, S.J. Braunhut, Biosens. Bioelectron. 16 (2001) 773–782.
[114] B. Zhang, Q. Mao, X. Zhang, T. Jiang, M. Chen, F. Yu, W. Fu, Biosens. Bioelectron. 19 (2004) 711–720.
[115] Y. Luo, M. Chen, Q. Wen, M. Zhao, B. Zhang, X. Li, F. Wang, Q. Huang, C. Yao, T. Jiang, G. Cai, W. Fu, Clin. Chem. 52 (2006) 2273–2280.
[116] J.B. Schlenoff, M. Li, H. Ly, J. Am. Chem. Soc. 117 (1995) 12528–12536.
[117] M.H. Schoenfisch, J.E. Pemberton, J. Am. Chem. Soc. 120 (1998) 4502–5413.
[118] M.D. Malinsky, K.L. Kelly, G.C. Schatz, R.P. Van Duyne, J. Am. Chem. Soc. 123 (2001) 1471–1482.
[119] W. Wang, T. Lee, M.A. Reed, Phys. Rev. B: Condens. Matter Mater. Phys. 68 (2003) 354161–354167.
[120] H. Ogi, H. Nagai, Y. Fukunishi, T. Yanagida, M. Hirao, M. Nishiyama, Anal. Chem. 82 (2010) 3957–3962.
[121] T. Kallio, S. Alajoki, V. Pore, M. Ritala, J. Laine, M. Leskelä, P. Stenius, Colloids Surf. A 291 (2006) 162–176.
[122] H. Hidaka, H. Honjo, S. Horikoshi, N. Serpone, Sens. Actuators B 123 (2007) 822–828.
[123] A. Fujishima, T.N. Rao, D.A. Tryk, J. Photochem. Photobiol. C 1 (2000) 1–21.
[124] L. Chen, Y. Guan, B. Yang, D. Shen, Prog. Chem. 14 (2002) 68–76.
[125] D. Grieshaber, R. MacKenzie, J. Vörös, E. Reimhult, Sensors 8 (2008) 1400–1458.